Electrically controlled nuclear polarization of individual atoms

Kai Yang[1], Philip Willke[1,2,3], Yujeong Bae[1,2,3], Alejandro Ferrón[4], Jose L. Lado[5,6], Arzhang Ardavan[7], Joaquín Fernández-Rossier[5,8], Andreas J. Heinrich[2,3,*], and Christopher P. Lutz[1,*]

[1]IBM Almaden Research Center, San Jose, CA 95120, USA
[2]Center for Quantum Nanoscience, Institute for Basic Science (IBS), Seoul 03760, Republic of Korea
[3]Department of Physics, Ewha Womans University, Seoul 03760, Republic of Korea
[4]Instituto de Modelado e Innovación Tecnológica (CONICET-UNNE), and Facultad de Ciencias Exactas, Naturales y Agrimensura, Universidad Nacional del Nordeste, Avenida Libertad 5400, W3404AAS Corrientes, Argentina
[5]QuantaLab, International Iberian Nanotechnology Laboratory (INL), Avenida Mestre José Veiga, 4715-310 Braga, Portugal
[6]Institute for Theoretical Physics, ETH Zurich, 8093 Zurich, Switzerland
[7]Clarendon Laboratory, Department of Physics, University of Oxford, Oxford OX1 3PU, UK.
[8]Departamento de Física Aplicada, Universidad de Alicante, San Vicente del Raspeig 03690, Spain

* Corresponding authors: A.J.H. (heinrich.andreas@qns.science) and C.P.L. (cplutz@us.ibm.com)

Nuclear spins are sensitive probes in analytical chemistry[1,2] and materials science[3,4] as well as promising candidates for quantum information processing[5-9]. Manipulating nuclear spins in condensed matter systems[5-7,10,11] is difficult due to the small nuclear magnetic moment, leading to low polarizations, and addressing them individually is particularly challenging[6,7,12]. Here, we polarize nuclear spins of individual copper (Cu) atoms on a surface using spin-polarized current in a scanning tuneling microscope. By employing the electron-nuclear flip-flop hyperfine interaction, the spin angular momentum is transferred to the nucleus of individual Cu atoms. The direction and magnitude of the nuclear polarization is controlled by the direction and amplitude of the current. We drive resonant transitions between polarized nuclear spin states, which can be used to sense the local magnetic environment of the Cu electron spin. This nuclear spin-transfer torque effect should be also present in other electrically accessible nuclear spin systems[6-8] such as the nuclear spins embedded in single-molecule magnets[6], and thus offers a general route towards electrically-controlled nuclear spin devices.

Nuclear magnetic resonance (NMR) is a powerful tool for probing local magnetic environments in condensed matter systems, ranging from magnetic ordering in high temperature superconductors[13,14] and spin liquids[15], to low-dimensional quantum magnetism in nanomagnets containing exchange-coupled ions[16,17]. Increasing the sensitivity and spatial resolution of NMR spectroscopy to the atomic scale requires strongly polarizing a single or a few nuclear spins, as well as driving and detecting them individually. However, the tiny magnetic moments of nuclear spins yield only weak thermal polarization. In 1953, Overhauser proposed that nuclear spin polarization exceeding the thermal equilibrium value, known as hyperpolarization, can be achieved through hyperfine coupling with electron spins[4,18]. The fundamental mechanism is the conservation of

angular momentum: electron spin "flips" and nuclear spin "flops", so that angular momentum is transferred from the electron to the nucleus. Such hyperpolarization, first achieved by saturating electron spin resonance in metals using microwave fields[4], enables applications such as *in vivo* magnetic resonance imaging using nanoparticles[19]. In the context of spin-based quantum information processing, ensemble ($\sim 10^5$ spins) hyperpolarization using optical pumping has been widely used in quantum dots[9] and ^{31}P doped silicon[10,20,21].

Electrical control of nuclear spins can be achieved using alternating[6,8] or static[11] electric fields, as well as electric current[22,23]. Compared to magnetic[7] and optical control[12], electrical control is particularly appealing for applications, because electric fields are relatively easy to generate locally and allow individual spins to be addressed[6]. Here, we use electric current to control nuclear magnetism of individual atoms for the first time. We demonstrate all-electric polarization and resonant driving of the single nuclear spin of a Cu atom by using a scanning tunneling microscope (STM) (Fig. 1a). The Cu nuclear spin is polarized with either polarity, by as much as 30%, which is ~17 times greater than thermal polarization at 1 K. This is achieved by employing a spin-transfer torque effect at the single-atom level (Fig. 1b). The current-controlled nuclear polarization permits detection of NMR, which is then used to sense the magnetic environment of the Cu atom.
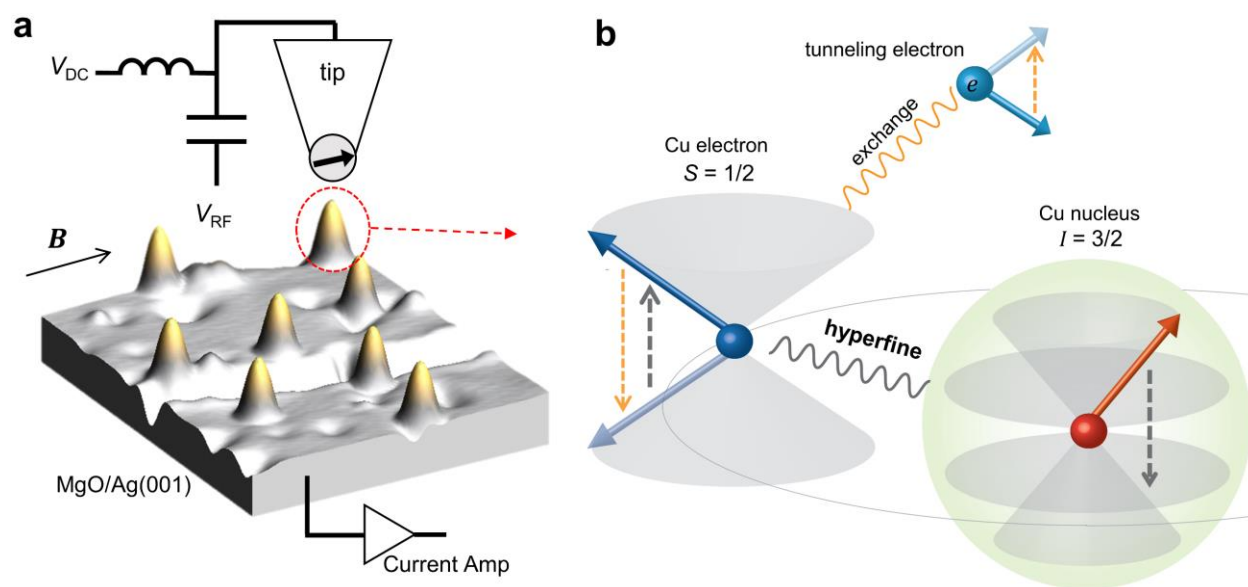

Figure 1 | Electrical polarization of the nuclear spin of a Cu atom on MgO. a, Schematic of the experimental set-up consisting of an STM with ESR capability, with an STM image of Cu atoms (yellow peaks) on bilayer MgO on Ag(001) (setpoint: V_{DC} = 50 mV, I_{DC} = 20 pA). Both DC (V_{DC}) and radio-frequency voltages (V_{RF}) are applied to the STM junction. Arrow at tip apex indicates a magnetic atom to give spin-polarized tip. **b**, Mechanism of the nuclear spin polarization for the coupled electron (S = 1/2) and nuclear (I = 3/2) spin system. The tunneling electron changes the orientation of the Cu electron spin by exchange interaction (dashed orange arrows), and angular momentum is subsequently transferred from the Cu electron to the Cu nucleus by the flip-flop hyperfine interaction (dashed grey arrows).

2

The Cu atoms were deposited on a MgO decoupling layer grown on a Ag(001) substrate (Fig. 1a). This set-up makes individual Cu atoms electrically accessible to the probe tip of STM, by measuring the time-average current (I_{DC})[24]. Each Cu atom adsorbs on top of the oxygen site (Fig. S1a), and has an electron spin $S = 1/2$ as determined below. Cu occurs naturally in two stable isotopes[25]: ^{63}Cu (~69%) and ^{65}Cu (~31%), and both have a nuclear spin $I = 3/2$. We model the coupled electron-nuclear system of Cu ($S = 1/2$, $I = 3/2$) in a magnetic field **B** by using an isotropic hyperfine coupling term and electron Zeeman term:

$$H = A\mathbf{S} \cdot \mathbf{I} + \gamma_e \mathbf{B} \cdot \mathbf{S}$$

Here A is the hyperfine constant and γ_e is the electron gyromagnetic ratio. The anisotropic components of the hyperfine coupling and electric quadrupole coupling are much weaker (< 100 MHz according to density functional theory (DFT) calculations in Supplementary Sec. 2), and are omitted here, as is the nuclear Zeeman energy.

We probe the quantum states of individual Cu atom by using inelastic electron tunneling spectroscopy (IETS)[26] and electron spin resonance (ESR)[27-29]. An in-plane magnetic field is applied to set the electron Zeeman energy of Cu. IETS reveals spin excitations between states with electron spin quantum number $m_S = \pm 1/2$ (labeled as ↑ and ↓ in the following), by measuring differential conductance (dI/dV) spectra (Fig. 2a). By fitting the electron Zeeman splitting as a function of B field (Fig. 2a, inset)[30], we obtain an electron g factor of 1.98 ± 0.10, and $\gamma_e = g\mu_B/h = 27.71 \pm 1.40$ GHz/T (h is the Planck's constant and μ_B is the Bohr magneton). This suggests that Cu has an electron spin $S = 1/2$, as confirmed by our DFT calculations.

We resolve the hyperfine structure of individual Cu atom by ESR[27,29], with an energy resolution of ~100 neV. Using a spin-polarized tip (Fig. S3a), we drive and detect the ESR transitions between ↑ and ↓ states of Cu. The four ESR peaks (Fig. 2b) correspond to the four different orientations of the nuclear spin $I = 3/2$ (Fig. 2d). The hyperfine constant A can be extracted from the four ESR frequencies: $A = (f_{II} + f_{IV} - f_I - f_{III})/2$ (Supplementary Sec. 6). The histogram of A values for 31 individual Cu atoms (Fig. 2b, right inset) shows two separate Gaussian peaks at 2.86 ± 0.03 GHz and 3.05 ± 0.07 GHz, corresponding to the two isotopes ^{63}Cu and ^{65}Cu, respectively. The ratio of 0.93 ± 0.02 between the two A values agrees well with the ratio of 0.9336 measured by the atomic beam technique[25]. This demonstrates the capability of ESR-STM to distinguish different isotopes with atomic precision, even when the nuclear spin magnitude is equal.

The hyperfine constant is sensitive to the chemical environment of an atom[29,31] and here the bonding configuration of Cu on MgO. DFT calculations revealed that the electron spin occupies mainly (~60 %) the 4s orbital (Fig. 2b, left inset). The large hyperfine constant of Cu on MgO, compared to

in other environments[31], thus arises from the large *s*-electron density at the nucleus, which yields an unusually large Fermi contact interaction[4]. The DFT calculated values for the two isotopes (A = 3.76 GHz and 4.02 GHz) agree well with the experimental values.
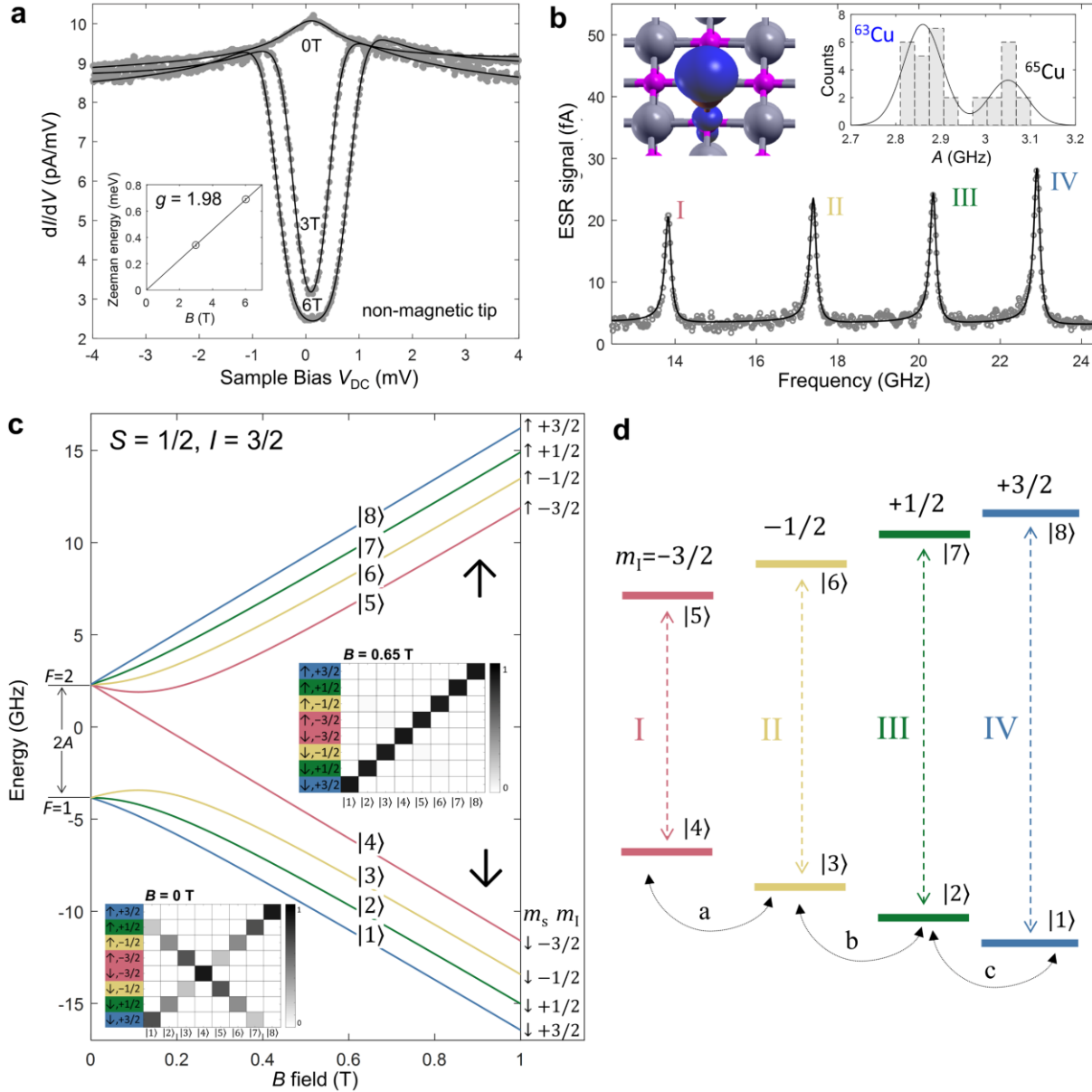

Figure 2 | Electronic and hyperfine structures of a single Cu atom on MgO. a, dI/dV spectra of Cu at different magnetic fields with a non-magnetic tip (setpoint: V_{DC} = 10 mV, I_{DC} = 100 pA; T = 0.6 K). Spectra are vertically shifted for clarity. The position of the conductance steps reveals the Zeeman energy. The zero-bias peak at zero field is a Kondo resonance. Inset: magnetic field dependence of the Zeeman energy. Linear fit constrained to zero Zeeman energy at zero field yields a g factor of 1.98 ± 0.10. **b**, ESR spectrum of a ^{65}Cu atom (setpoint: V_{DC} = −20 mV, I_{DC} = 40 pA; V_{RF} = 15 mV, total field B = 0.65 T consisting of an external field of 0.765 T and an effective tip field, T = 1.2 K). Inset: (Left) Calculated spin density (dark blue) of Cu on MgO. (Right) Histogram of hyperfine constant A of 31 Cu atoms, fit by two Gaussians. **c**, Energy diagram of the electron-

nuclear spin system as a function of B field. Insets: Schematic of the energy eigenstates at $B = 0$ and 0.65 T. Each column represents one eigenstate. The grey level represents the probability amplitudes in the basis of Zeeman product states $|m_S, m_I\rangle$, where $m_S = \uparrow, \downarrow$ and $m_I = \pm 3/2, \pm 1/2$. At zero field, the eight eigenstates consist of a triplet (total spin $F = 1$) and a quintet ($F = 2$). At 0.65 T, the eight eigenstates are nearly Zeeman product states [see eq. (S3)]. Note that states $|\downarrow, -3/2\rangle$ ($|4\rangle$) and $|\uparrow, +3/2\rangle$ ($|8\rangle$) are exact eigenstates for all values of B field. **d**, Schematic energy level diagram at 0.65 T showing ESR (vertical arrows) and NMR (arc arrows) transitions, labeled by I-IV and a-c respectively.

We plot the energy diagram of a Cu atom in Fig. 2c. The eight eigenstates are labelled as $|i\rangle$ ($i = 1$ to 8). In the limit of high B field (electron Zeeman energy much larger than hyperfine coupling), the eigenstates are nearly the Zeeman product states $|m_S, m_I\rangle$, where $m_S = \uparrow, \downarrow$ and $m_I = \pm 3/2, \pm 1/2$. In general, the state $|\downarrow, m_I\rangle$ hybridizes with $|\uparrow, m_I -1\rangle$ ($m_I = +3/2, \pm 1/2$) due to the flip-flop hyperfine interaction ($S^+ I^-$ and $S^- I^+$), to form three pairs of hybrid states ($|i\rangle$ and $|8 - i\rangle$ with $i = 1, 2, 3$)[5]. For example, at $B = 0.65$ T, the Zeeman energy is ~ 6 times larger than the hyperfine coupling for both isotopes, and states $|\downarrow, +3/2\rangle$ and $|\uparrow, +1/2\rangle$ mix to form $|1\rangle \approx 0.99|\downarrow, +3/2\rangle - 0.12|\uparrow, +1/2\rangle$ and $|7\rangle \approx 0.12|\downarrow, +3/2\rangle + 0.99|\uparrow, +1/2\rangle$. Due to the slight overlap between eigenstates $|i\rangle$ and $|8 - i\rangle$ ($|\langle i|S_z|8 - i\rangle|^2 \neq 0$), tunneling electrons can induce state transitions by scattering with the Cu electron, during which the spin of the tunneling electron is conserved ($\Delta\sigma = 0$). In comparison, $\Delta\sigma = \pm 1$ transitions (tunneling electron reverses its spin) can occur between $|i\rangle$ and $|9 - i\rangle$ since $|\langle i|S_x|9 - i\rangle|^2 \neq 0$. We use these two types of current-induced transitions to control the nuclear polarization as shown below.

The nuclear polarization, $P_n = \langle I_z \rangle / I$, is only $\sim 1.7\%$ for ^{63}Cu or ^{65}Cu at thermal equilibrium ($B = 0.65$ T, $T = 1.2$ K). This polarization results from the Boltzmann occupation of nuclear sub-states that are separated by only $\sim A/2$. The main thermal relaxation path is likely through scattering by electrons from the Ag substrate[24,32].

We control the nuclear polarization P_n using a spin-polarized current flowing through individual Cu, while the readout of P_n is simultaneously realized by taking ESR spectra. Note that the ESR-induced transition rate is much smaller than the current-induced rates (Fig. S5) and thus the ESR process only weakly perturbs P_n. Figures 3a and 3b show the ESR spectra taken with spin-polarized currents of opposite directions given by opposite bias polarities. The relative amplitudes of the ESR peaks directly reveal the steady-state populations of each nuclear spin state at large I_{DC}. We find that sufficiently large negative bias (electrons tunnel from sample to tip), and thus large current when holding the tip height constant, leads to nuclear spin polarization primarily into the $m_I = -3/2$ states (Fig. 3a). Reversing the current direction by applying positive bias leads to a higher occupation of the $m_I = +3/2$ states (Fig. 3b). Figure 3c shows the ESR amplitudes as a function of sample bias V_{DC} at

constant tip height. Increasing V_{DC} and thus the current I_{DC} increases the degree of nuclear polarization, which saturates to a limiting polarization at large I_{DC}.
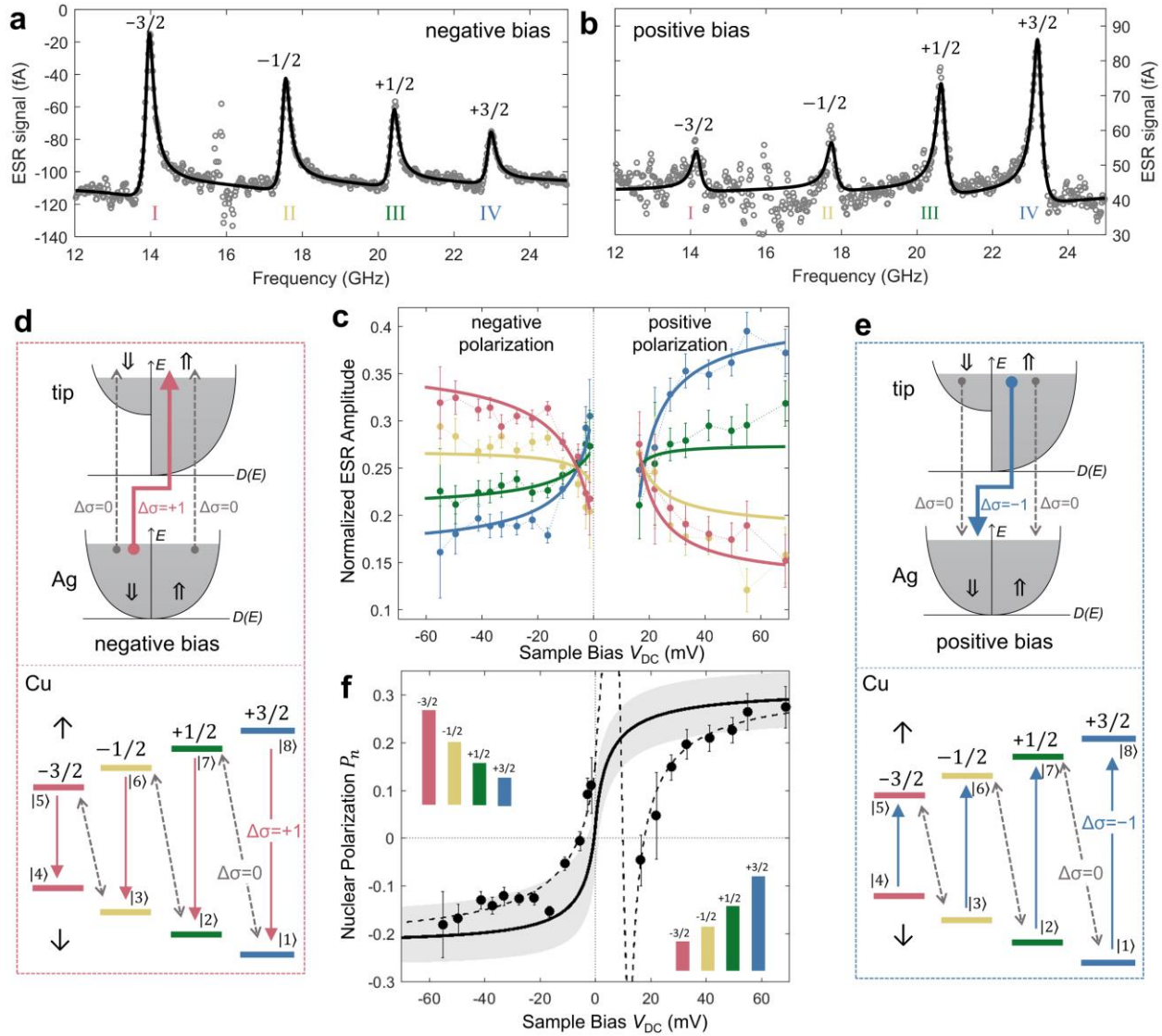

Figure 3 | Spin-transfer torque of the Cu nuclear spin. **a** and **b**, ESR spectra of a ^{65}Cu atom at $V_{DC} = -22$ mV and $+22$ mV for the same tip ($I_{DC} = 60$ pA, $V_{RF} = 12$ mV, total field $B = 0.66$ T consisting of an external field of 0.74 T and an effective tip field, $T = 1.2$ K). **c**, Normalized ESR amplitudes as a function of sample bias measured with a different tip than in (a, b) (setpoint: $V_{DC} = 22$ mV, $I_{DC} = 80$ pA; $V_{RF} = 6–20$ mV, $B = 0.66$ T, $T = 1.2$ K). Negative and positive sides are fit separately using the rate equation model (see eq. (S15)), giving a tip polarization η of 0.14 (0.19) at negative (positive) bias. **d**, Mechanism of the nuclear polarization at negative bias ($V_{DC} < 0$). Upper panel: $\Delta\sigma = +1$ (red arrow) and $\Delta\sigma = 0$ (dashed grey arrows) electron tunneling. Lower panel: $\Delta\sigma = +1$ tunneling drives the Cu electron spin from $m_S = \uparrow$ to $\downarrow$ (red arrows); $\Delta\sigma = 0$ tunneling drives the flip-flop transitions (dashed grey arrows). The magnetic tip here is anti-aligned with the ground-state Cu electron spin. Oppositely aligned tip torques the nuclear spin in the opposite directions (see Fig. S3). The weaker tunneling process having opposite spin-flip sign ($\Delta\sigma = -1$) is also present (not pictured). **e**, Mechanism of the nuclear polarization at positive bias ($V_{DC} > 0$). The weaker tunneling process ($\Delta\sigma = +1$) is also present (not pictured). **f**, Nuclear polarization P_n as a function of V_{DC} (solid curve), based on fits to results in (c) using

the rate equation model. The uncertainty of P_n is depicted as the shaded region by considering the uncertainties of the fitting parameters with 95% confidence. Dashed curve is the asymmetry in ESR peak amplitudes calculated from the same model [see eq. (S17)]. The asymmetry approaches P_n in the limit of large bias, but deviates from the true nuclear polarization at small current. Data points are the measured asymmetry obtained directly by weighting the four ESR amplitudes of the same V_{DC} in (c). The error bars are propagated from the fitting uncertainties of the ESR peak amplitudes at each V_{DC}.

The current-controlled nuclear polarization is a consequence of the conservation of total spin angular momentum through two spin-transfer torque[33] processes at the single-atom level (Fig. 1b). The principle is illustrated in Figs. 3d and 3e for each bias polarity. For example, at positive V_{DC}, tunneling electrons firstly exchange spin angular momentum with the localized Cu electron spin by exchange scattering (blue arrow in the upper panel of Fig. 3e). This spin-reversing ($\Delta\sigma = -1$) electron tunneling pumps the electron spin of the Cu atom from the four lower states to the upper states ($\Delta m_S = +1$) to conserve angular momentum[32]. At large I_{DC}, the population ratio between the two states with the same m_I (between $|i\rangle$ and $|9-i\rangle$) is set by the spin polarization (η) of the tip, to give a ratio of $(1+\eta)/(1-\eta)$, where $\eta \approx 0.19$ for this tip (from the fit in Fig. 3c). The second step of the spin-transfer torque occurs between the nuclear and electron spins of the Cu atom via the flip-flop hyperfine interaction (S^+I^- and S^-I^+). At large I_{DC}, this process is mainly driven by the spin-conserving ($\Delta\sigma = 0$) electron tunneling events (dashed grey arrows in Fig. 3e), which equalize the populations of the connected states ($|i\rangle$ and $|8-i\rangle$). At low I_{DC}, scattering of electrons from the Ag substrate sets the Boltzmann distribution of the connected states.

Considering all transitions, the state population at positive V_{DC} follows the paths indicated by the arrows in Fig. 3e, and the net effect is that the nuclear spin is driven towards the states $|1\rangle$ and $|8\rangle$, which are mainly composed of $m_I = +3/2$, giving positive nuclear spin polarization P_n. Similarly, at negative sample bias, the populations are driven to $m_I = -3/2$ states (Fig. 3d), giving negative P_n.

To quantitatively describe the behavior of the electron and nuclear spin of Cu under the influence of the spin-polarized current, we developed a rate equation model (Supplementary Sec. 6). This model considers transition rates between states due to scattering with electrons that tunnel between tip and Ag, as well as scattering by Ag substrate electrons (originating from Ag and returning to Ag), using a quantum mechanical transition intensity operator[32]. We treat the ESR-induced rates as perturbations (Fig. S5). By fitting the ESR amplitudes versus V_{DC} in Fig. 3c to our model, we obtained the nuclear polarization P_n at different V_{DC} (Fig. 3f, solid curve). At large current, P_n can also be approximated from the ratios of the four ESR amplitudes at each V_{DC} (see dashed curve in Fig. 3f and Supplementary Sec. 7). The ESR amplitudes (Fig. 3c) along with the corresponding calculated P_n (Fig. 3f, dashed curve) show an asymmetry with respect to zero bias, due to different spin pumping directions at opposite bias polarities. At positive V_{DC}, thermal relaxation due to substrate electrons,

The model shows that P_n grows monotonically with V_{DC} and the polarization direction is controlled by the bias polarity. The result is a fast electrical initialization of the nuclear spin. We find that when the exchange scattering with tunneling electrons occurs more frequently than the spin relaxation driven by substrate electrons (every ~10 ns as estimated from the point contact conductance[24]), the nuclear spin population starts to deviate from the thermal equilibrium. The saturation polarization at +70 mV is ~30%, which is a ~17-fold enhancement over the thermal equilibrium. This corresponds to an effective nuclear spin temperature of ~200 mK, which is 6 times cooler than the experimental temperature of 1.2 K. The model also shows that the saturation polarization increases monotonically with the tip spin polarization, and reaches unity with a fully polarized tip (η = 1) (Fig. S4). The time needed to reach the steady-state polarization is limited by the rates of the flip-flop transitions (Δσ = 0), which are slower than the Δσ = ±1 transitions by a factor of $\alpha = (\gamma_e B / A)^2 \approx 40$. The settling time is thus ~4α·(e/I_{DC}) = 420 ns at I_{DC} of 60 pA[32].
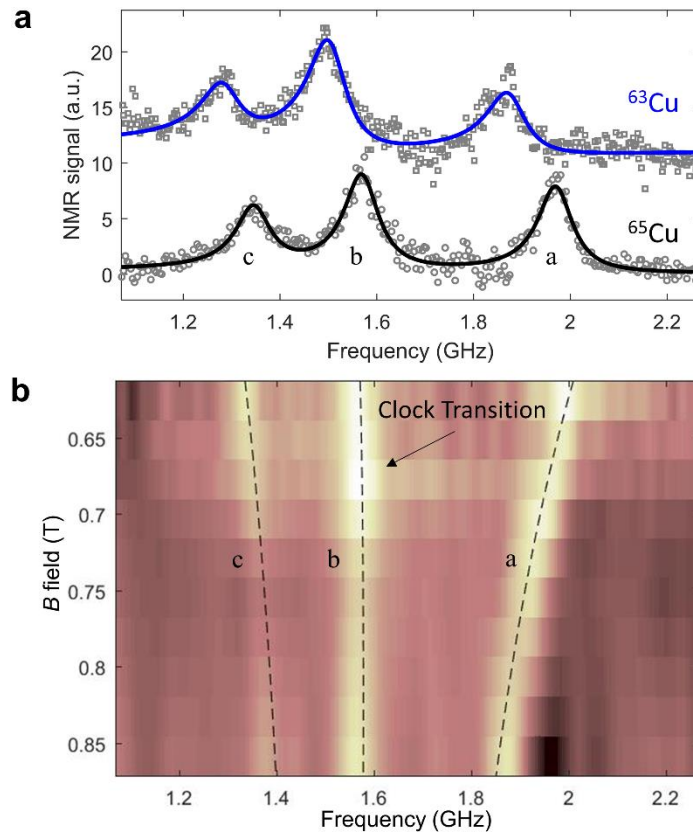

Figure 4 | NMR-type transitions of single Cu atoms. a, NMR spectra of single [63]Cu and [65]Cu atoms on MgO (setpoint: V_{DC} = −22 mV, I_{DC} = −60 pA; V_{RF} = 25 mV, B = 0.66 T, T = 1.2 K). Transitions are labeled as in Fig. 2d,

and detected by the change of the magneto-resistance of the electron states using the DC current, different than the traditional double resonance technique (see Fig. S6 for double resonance spectra)[4]. Transitions between upper four states ($m_S = \uparrow$) may also contribute to the spectrum, but these should be much weaker due to their small populations at this spin torque polarity. Solid lines are the fit to three Lorentzian peaks. Spectra are vertically shifted for clarity. **b**, NMR spectra of a ^{65}Cu atom as a function of total B field (setpoint: V_{DC} = 16–22 mV, I_{DC} = 60 pA). The total B field is varied by changing the tip field at an external field of 0.74 T. The values of the total B field are obtained by measuring the ESR spectra of Cu for each tip position. Dashed lines are the calculated transition frequencies.

The polarized nuclear spin permits direct access to the resonant transitions between adjacent nuclear spin states[4,34] (changing m_I and leaving m_s unchanged) at the single atom scale (Fig. 4a). These NMR-type transitions[35] (labeled NMR in the following for brevity) are driven by an AC voltage applied at one of the transition frequencies ($\sim A/2$), and are likely made possible by the mixing of electron and nuclear states (Supplementary Sec. 6)[5]. The resonances are detected by the change of electron spin polarization (and thus the magneto-resistance) that results from the NMR transitions. The NMR spectrum of single Cu atoms reveals three peaks, corresponding to transitions a–c labeled in Fig. 2d. The separation of NMR frequencies makes it possible to individually address each transition. The uneven spacing of nuclear states is due to the hyperfine coupling. The relatively broad NMR peaks compared to other nuclear spin systems[6-8] are due to a shorter nuclear coherence time, which is limited by the electron spin relaxation time resulting from the interaction with the tunneling current as well as the scattering electrons from the Ag substrate.

We employ the NMR spectra to probe the local magnetic environment of a ^{65}Cu atom by varying the effective tip magnetic field[28] applied to the atom. The change of the Zeeman energy of the Cu electron spin manifests as an NMR frequency shift (Fig. 4b). Two frequencies (a and c) shift with the tip magnetic field while the frequency of b is almost constant at $\sim$1.6 GHz, which agrees well with the calculated evolution (dashed lines in Fig. 4b). The transition b is an NMR-type clock transition[35,36], a transition that is insensitive to the B field. The clock transition of ^{63}Cu occurs at a smaller frequency of $\sim$1.5 GHz (Fig. 4a) due to its smaller hyperfine constant. The clock transition frequency can thus be used to distinguish two Cu isotopes.

The nuclear spin-transfer torque effect shown here should be applicable to other electron-nuclear quantum devices with nuclear spins coupled to unpaired electrons[5-8]. Although the nuclear spin relaxation time of Cu on MgO is not yet long enough to perform single-shot readout of nuclear spin states, it should be possible to improve this by using a thicker MgO layers or by using Cu-based molecules[37]. The electrical polarization, driving, and detection of the nuclear spin states provides a new means of local spin manipulation for nuclear spintronics[34] and detection of the atomic-scale magnetic environment in nanomagnets[16,17].

References

1   T. Staudacher, F. Shi, S. Pezzagna, J. Meijer, J. Du, C. A. Meriles, F. Reinhard & J. Wrachtrup. Nuclear magnetic resonance spectroscopy on a (5-nanometer)[3] sample volume. *Science* **339**, 561-563 (2013).

2   F. Shi, Q. Zhang, P. Wang, H. Sun, J. Wang, X. Rong, M. Chen, C. Ju, F. Reinhard, H. Chen, J. Wrachtrup, J. Wang & J. Du. Single-protein spin resonance spectroscopy under ambient conditions. *Science* **347**, 1135-1138 (2015).

3   M. Fu, T. Imai, T.-H. Han & Y. S. Lee. Evidence for a gapped spin-liquid ground state in a kagome Heisenberg antiferromagnet. *Science* **350**, 655-658 (2015).

4   C. P. Slichter. *Principles of magnetic resonance.* (Springer, 1996).

5   G. W. Morley, P. Lueders, M. Hamed Mohammady, S. J. Balian, G. Aeppli, C. W. M. Kay, W. M. Witzel, G. Jeschke & T. S. Monteiro. Quantum control of hybrid nuclear–electronic qubits. *Nat. Mater.* **12**, 103-107 (2013).

6   S. Thiele, F. Balestro, R. Ballou, S. Klyatskaya, M. Ruben & W. Wernsdorfer. Electrically driven nuclear spin resonance in single-molecule magnets. *Science* **344**, 1135-1138 (2014).

7   J. J. Pla, K. Y. Tan, J. P. Dehollain, W. H. Lim, J. J. L. Morton, F. A. Zwanenburg, D. N. Jamieson, A. S. Dzurak & A. Morello. High-fidelity readout and control of a nuclear spin qubit in silicon. *Nature* **496**, 334-338 (2013).

8   A. J. Sigillito, A. M. Tyryshkin, T. Schenkel, A. A. Houck & S. A. Lyon. All-electric control of donor nuclear spin qubits in silicon. *Nat. Nanotechnol.* **12**, 958-962 (2017).

9   B. Urbaszek, X. Marie, T. Amand, O. Krebs, P. Voisin, P. Maletinsky, A. Högele & A. Imamoglu. Nuclear spin physics in quantum dots: An optical investigation. *Rev. Mod. Phys.* **85**, 79-133 (2013).

10   D. R. McCamey, J. van Tol, G. W. Morley & C. Boehme. Fast nuclear spin hyperpolarization of phosphorus in silicon. *Phys. Rev. Lett.* **102**, 027601 (2009).

11   J. H. Smet, R. A. Deutschmann, F. Ertl, W. Wegscheider, G. Abstreiter & K. von Klitzing. Gate-voltage control of spin interactions between electrons and nuclei in a semiconductor. *Nature* **415**, 281 (2002).

12   M. V. G. Dutt, L. Childress, L. Jiang, E. Togan, J. Maze, F. Jelezko, A. S. Zibrov, P. R. Hemmer & M. D. Lukin. Quantum register based on individual electronic and nuclear spin qubits in diamond. *Science* **316**, 1312-1316 (2007).

13   H. Alloul, T. Ohno & P. Mendels. ^{89}Y NMR evidence for a fermi-liquid behavior in $YBa_2Cu_3O_{6+x}$. *Phys. Rev. Lett.* **63**, 1700-1703 (1989).

14   T. Wu, H. Mayaffre, S. Krämer, M. Horvatić, C. Berthier, W. N. Hardy, R. Liang, D. A. Bonn & M.-H. Julien. Magnetic-field-induced charge-stripe order in the high-temperature superconductor $YBa_2Cu_3O_y$. *Nature* **477**, 191 (2011).

15   P. Mendels, A. Keren, L. Limot, M. Mekata, G. Collin & M. Horvatić. Ga NMR study of the local susceptibility in kagomé-based $SrCr_8Ga_4O_{19}$: Pseudogap and paramagnetic defects. *Phys. Rev. Lett.* **85**, 3496-3499 (2000).

16   F. Borsa, A. Lascialfari & Y. Furukawa. NMR in Magnetic Molecular Rings and Clusters. In: *Novel NMR and EPR techniques* (pp. 297-349, eds Janez Dolinšek, Marija Vilfan, & Slobodan Žumer, Springer Berlin Heidelberg, 2006).

17   E. Micotti, Y. Furukawa, K. Kumagai, S. Carretta, A. Lascialfari, F. Borsa, G. A. Timco & R. E. P. Winpenny. Local spin moment distribution in antiferromagnetic molecular rings probed by NMR. *Phys. Rev. Lett.* **97**, 267204 (2006).

18   A. W. Overhauser. Polarization of nuclei in metals. *Phys. Rev.* **92**, 411-415 (1953).

19   M. C. Cassidy, H. R. Chan, B. D. Ross, P. K. Bhattacharya & C. M. Marcus. *In vivo* magnetic resonance imaging of hyperpolarized silicon particles. *Nat. Nanotechnol.* **8**, 363 (2013).

20   S. Simmons, R. M. Brown, H. Riemann, N. V. Abrosimov, P. Becker, H.-J. Pohl, M. L. W. Thewalt, K. M. Itoh & J. J. L. Morton. Entanglement in a solid-state spin ensemble. *Nature* **470**, 69 (2011).

21   G. W. Morley, M. Warner, A. M. Stoneham, P. T. Greenland, J. van Tol, C. W. M. Kay & G. Aeppli. The initialization and manipulation of quantum information stored in silicon by bismuth dopants. *Nat. Mater.* **9**, 725 (2010).

22   C. C. Lo, C. D. Weis, J. van Tol, J. Bokor & T. Schenkel. All-electrical nuclear spin polarization of donors in silicon. *Phys. Rev. Lett.* **110**, 057601 (2013).

23   C. J. Trowbridge, B. M. Norman, Y. K. Kato, D. D. Awschalom & V. Sih. Dynamic nuclear polarization from current-induced electron spin polarization. *Phys. Rev. B* **90**, 085122 (2014).

24   W. Paul, K. Yang, S. Baumann, N. Romming, T. Choi, C. P. Lutz & A. J. Heinrich. Control of the millisecond spin lifetime of an electrically probed atom. *Nat. Phys.* **13**, 403-407 (2017).

25   Y. Ting & H. Lew. Hyperfine structure of Cu^{63} and Cu^{65}. *Phys. Rev.* **105**, 581-588 (1957).

26   A. J. Heinrich, J. A. Gupta, C. P. Lutz & D. M. Eigler. Single-atom spin-flip spectroscopy. *Science* **306**, 466-469 (2004).

27   S. Baumann, W. Paul, T. Choi, C. P. Lutz, A. Ardavan & A. J. Heinrich. Electron paramagnetic resonance of individual atoms on a surface. *Science* **350**, 417-420 (2015).

28   K. Yang, Y. Bae, W. Paul, F. D. Natterer, P. Willke, J. L. Lado, A. Ferrón, T. Choi, J. Fernández-Rossier, A. J. Heinrich & C. P. Lutz. Engineering the eigenstates of coupled spin-1/2 atoms on a surface. *Phys. Rev. Lett.* **119**, 227206 (2017).

29   P. Willke, Y. Bae, K. Yang, J. L. Lado, A. Ferrón, T. Choi, A. Ardavan, J. Fernández-Rossier, A. J. Heinrich & C. P. Lutz. Hyperfine interaction of individual atoms on a surface. *Submitted* (2018).

30   A. F. Otte, M. Ternes, K. von Bergmann, S. Loth, H. Brune, C. P. Lutz, C. F. Hirjibehedin & A. J. Heinrich. The role of magnetic anisotropy in the Kondo effect. *Nat. Phys.* **4**, 847-850 (2008).

31   B. R. McGarvey. The isotropic hyperfine interaction. *J. Phys. Chem.* **71**, 51-66 (1967).

32   S. Loth, K. von Bergmann, M. Ternes, A. F. Otte, C. P. Lutz & A. J. Heinrich. Controlling the state of quantum spins with electric currents. *Nat. Phys.* **6**, 340-344 (2010).

33   A. Brataas, A. D. Kent & H. Ohno. Current-induced torques in magnetic materials. *Nat. Mater.* **11**, 372 (2012).

34   J. A. Reimer. Nuclear hyperpolarization in solids and the prospects for nuclear spintronics. *Solid State Nucl. Magn. Reson.* **37**, 3-12 (2010).

35   G. Wolfowicz, A. M. Tyryshkin, R. E. George, H. Riemann, N. V. Abrosimov, P. Becker, H.-J. Pohl, M. L. W. Thewalt, S. A. Lyon & J. J. L. Morton. Atomic clock transitions in silicon-based spin qubits. *Nat. Nanotechnol.* **8**, 561-564 (2013).

36   M. Shiddiq, D. Komijani, Y. Duan, A. Gaita-Ariño, E. Coronado & S. Hill. Enhancing coherence in molecular spin qubits via atomic clock transitions. *Nature* **531**, 348-351 (2016).

37   B. W. Heinrich, L. Braun, J. I. Pascual & K. J. Franke. Protection of excited spin states by a superconducting energy gap. *Nat. Phys.* **9**, 765 (2013).

Acknowledgements

Author contributions

K.Y. and C.P.L. designed the experiment. K.Y., P.W., and Y.B. carried out the STM measurements. K.Y. and C.P.L. performed the analysis and developed the rate equation model. A.F., J.L.L. and J.F-R. performed the DFT calculations. All authors discussed the results and edited the manuscript.

Data availability

The data that support the plots within this paper and other findings of this study are available from the corresponding author upon reasonable request.